Available online at www.sciencedirect.com

ScienceDirect

journal homepage: www.elsevier.com/locate/he

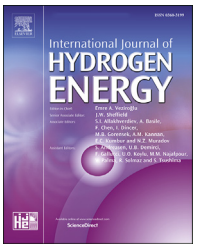

# Turbulent flame topology and the wrinkled structure characteristics of high pressure syngas flames up to 1.0 MPa

*Meng Zhang, Jinhua Wang*, Min Chang, Zuohua Huang***

*State Key Laboratory of Multiphase Flow in Power Engineering, Xi'an Jiaotong University, Xi'an 710049, China*

ARTICLE INFO

*Article history:*
Received 15 July 2018
Received in revised form
18 August 2018
Accepted 21 August 2018
Available online 24 September 2018

*Keywords:*
Syngas
Hydrogen ratio
Turbulent premixed flame
Turbulent flame topology
High pressure

ABSTRACT

The turbulent flame topology characteristics of the model syngas with two different hydrogen ratios were statistically investigated, namely $CO/H_2$ ratio at 65/35 and 80/20, at equivalence ratio of 0.7. The combustion pressure was kept at 0.5 MPa and 1.0 MPa, to simulate the engine-like condition. The model syngas was diluted with $CO_2$ with a mole fraction of 0.3 which mimics the flue gas recycle in the turbulent combustion. $CH_4$/air flame with equivalence ratio of 1.0 was also tested for comparison. The flame was anchored on a premixed type Bunsen burner, which can generate a controllable turbulent flow. Flame front, which is represented by the sharp increased interface of the OH radical distribution, was measured with OH-PLIF technique. Flame front parameters were obtained through image processing to interpret the flame topology characteristics. Results showed that the turbulent flames possess a wrinkled character with smaller scale concave/convex structure superimposed on a larger scale convex structure under high pressure. The wrinkled structure of syngas flame is much finer and more corrugated than hydrocarbon fuel flames. The main reason is that scale of wrinkled structure is smaller for syngas flame, resulting from the unstable physics. Hydrogen in syngas can increase the intensity of the finer structure. Moreover, the model syngas flames have larger flame surface density than $CH_4$/air flame, and hydrogen ratio in syngas can increase flame surface density. This would be mainly attributed to the fact that the syngas flames have smaller flame intrinsic instability scale $l_i$ than $CH_4$/air flame. $S_T/S_L$ of the model syngas tested in this study is higher than $CH_4$/air flames for both pressures, due to the high diffusivity and fast burning property of $H_2$. This is mainly due to smaller $L_M$ and $l_i$. $V_f$ of the two model syngas is much smaller than $CH_4$/air flames, which suggests that syngas flame would lead to a larger possibility to occur combustion oscillation.



## Introduction

The threat of energy crisis and global warming are two of the greatest challenges to mankind in the beginning of the third millennium. Exploring the environment friendly alternative fuels would be very urgent and of primary importance. A very prospective technology to burn coal and other wastes is called Integrated Gasification Combined Cycle (IGCC), which has been regarded as a very promising way due to its specific

* *Corresponding author.*
** *Corresponding author.*
E-mail addresses: jinhuawang@mail.xjtu.edu.cn (J. Wang), zhhuang@mail.xjtu.edu.cn (Z. Huang).
https://doi.org/10.1016/j.ijhydene.2018.08.154
0360-3199/

merits. For example, it can adapt diverse fuel and fit for the Carbon Capture and Storage (CCS) technique [1]. Moreover, with CCS technology IGCC can achieve high efficiency and low emissions, which is very economical to the energy and friendly to environment protection. The IGCC power plants can gasify a variety of liquid and solid fuel, such as coal, agricultural wastes. The gasified fuel is converted into a synthetic gas eventually, mentioned as syngas in the literature, which will be subsequently consumed in the combustion device, i.e. gas turbine. The syngas from IGCC mainly consists of CO, $H_2$ and the minor components are $CH_4$, $N_2$, $CO_2$, $H_2O$ and other hydrocarbons [2].

Hydrogen, considered as the most promising clean energy with great potential, has a very small and light molecular which leads to high reactivity, high diffusivity and fast chemical reaction, i.e. large laminar burning velocity [3]. These properties result in a fact that a small amount of hydrogen addition in other fuel, say $CH_4$ and CO, would have a catalytic effect on the combustion of the fuel [4]. As a consequence, the amount of $H_2$ in the syngas would change turbulence-flame interaction mechanism in a real combustion device, i.e. premixed-type gas turbine, which significantly influences the combustor performance, compared with the traditional hydrocarbon fuels [5] such as $CH_4$. Meanwhile, the mole fraction of every component in syngas varies significantly and highly depends on the fuel resources and production technology. According to Siemens' report, the mole fraction of $H_2$ can vary from 9.0% to 41.4% when the fuel of IGCC plant varies from coal to biomass or other solid wastes [6]. Even fueled with coal only, the percentage of hydrogen can vary from 25% to 70% depending on production technology [7].

Many researches have been conducted on premixed syngas flames, at both laminar and turbulent condition. Numerous studies were done on flame topology characteristics [8,9] and the instability [10,11], including thermal diffusive instability and hydrodynamic instability, of $CO/H_2$ mixed fuels and $CH_4$ under on laminar condition. And the corresponding experiments were also performed at high pressure [12,13], but there were few investigations on the turbulent case. Some previous work focusing on the premixed flame characteristics has been conducted in the configuration of the freely propagating spherical flame [14,15], Bunsen flame [16,17] or V shape flame [18] of $CH_4$/air mixture. However, due to the difficulties on experimental performance and controlling, studies on of syngas by means of continuous turbulent flames, such as Bunsen flame, under engine-like pressure are very limited. Moreover, when the fuel of IGCC was burned in premixed type with CCS, the unburned mixture was usually diluted by the exhausted gas recycled from the burned gas, in which the mole fraction of $CO_2$ is relatively high, aiming to decrease the flame temperature since the heat capacity of $CO_2$ is large.

Due to the unique property of hydrogen contained in syngas, both the unburned mixture and laminar flame present distinct behavior compared with conventional hydrocarbons flames, say methane/air flame. Those properties would significantly influence the chemical reaction process occurred in combustion, as a consequence affecting the turbulence-flame interaction when combustion was occurred in turbulent condition. This would cause the difference of turbulent flame characteristics between syngas and hydrocarbon flames, like flame front wrinkled structure and the fractal features, to be evident. Those characteristics describing turbulent flame can reveal the mechanism of the aforementioned turbulence-flame interaction [19] and, also, they are essential and of primary importance to the combustion modeling, especially at modern advanced combustor design, which needs to be further studied in details.

The objective of this study is to investigate the effect of hydrogen ratio on turbulence-flame interaction at high pressure by analyzing the flame topology and wrinkled structure of the turbulent Bunsen flame. Two syngas mixtures with different $CO/H_2$ mixing ratios and 30% $CO_2$ dilution ratio were investigated as the typical model syngas, representing the syngas obtained from different production technology. $CO_2$ was used to mimic the flue gas recycle. Turbulent flow field was measured and OH-PLIF technique was implemented for detecting the instantaneous turbulent premixed flames. The paper was organized as follows. Section Experimental setup and procedures introduce the experimental set-up and method. The results were presented and analyzed in Section Results and discussions and the work was summarized in Section Conclusions.

## Experimental setup and procedures

Turbulent flames were anchored on a Bunsen burner placed in a high-pressure combustion facility, which has been introduced elsewhere [4,20,21]. Several modules were utilized performing the experiments, i.e. the air supply system, the OH-PLIF laser detection system and the combustion device, namely the turbulent premixed Bunsen-type burner. A standard premixed type turbulent flame was generated with the burner which was placed inside a high pressure combustion chamber. The highly compressed air was dehumidified, dust extracted and then divided into two flows. A large quantity of the clean fresh compressed air is charged to the combustion chamber to preserve the target ambient pressure, in the other hand, to wash away the hot burned gases due to the large heat release during combustion [20]. A small portion of the fresh air was quantitatively controlled by mass flow meter as the oxidizer mixing with fuel. The unburned mixture charged to the burner was firstly impinged to a plate which was installed close to the inlet of the burner, for sufficient mixing. Then the mixture goes through two sintered metals, with different characteristic dimension, decreasing in order, to ensure a rectified and fully mixed unburned mixture, in the other hand to prevent flame propagating back. Various type perforated plates with different hole characteristic dimension and pass-through ratio were utilized to produce the turbulence with a wide range of intensity. The geometry of the perforated plates was shown in Fig. 1 and the characteristics was given in Table 1. A controllable turbulent flow can be produced and the turbulent flame was anchored at the burner nozzle, with a diameter of 20 mm. Moreover, a weak hydrogen diffusion pilot flame was served at a 0.5 mm annulus around the nozzle, to anchor the flame and to ensure safe ignition.

The instantaneous OH radical distribution, whose sharp increasing interface representing turbulent flame surface, was detected by OH-PLIF laser diagnostic technique, which has

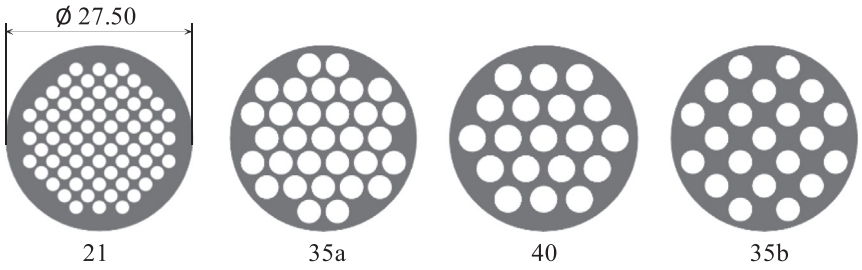


**Fig. 1 – Perforated plates used in this study.**

been introduced in detail in our previous work. We use a wavelength of 283.56 nm obtained from a flame test as the exciting wavelength, which can excite maximum OH radical. Secondly, we install an OH filter in the ICCD camera to keep the wavelength of 308 ± 10 nm to make sure fluorescence captured was from OH. Interested readers can refer [17,21]. A constant-temperature hot-wire anemometer (Dantec, Streamline 90 N) was utilized to measure the turbulent flow characteristics at burner exit. The measurement position was tested and was set 10 mm above the nozzle. The parameters describing turbulent flow, such as turbulence intensity, integral scale, Kolmogorov scale et al., were obtained by processing the original data with Taylor hypothesis and isotropic turbulence assumption. The data was obtained at various bulk velocities and multiple locations along burner diameter to avoid the large uncertainties due to the fluctuations nature of turbulence. Firstly, an $U_{ave}$ was set from the volume flow rate at burner exit, namely $U_{ave} = Q/\pi r^2$. Then, the instantaneous velocity was measured at different locations to calculate the local mean velocity $U_{local}$ and the root mean square of the fluctuation $u'$, which was regarded as turbulence intensity. Fig. 2 plotted the measured data for plate '35b' at two $U_{ave}$, i.e. 3 m/s and 5 m/s. The sensor was placed at different angle, i.e. 0°and 45°, with the incoming flow for validating the isotropic assumption. It can be seen that the $U_{ave}$ and $U_{local}$ are in the same magnitude for the two tested cases, which confirms the isotropic assumption. Moreover, the linearity of $u'$ with respect to the averaged velocity was plotted in Fig. 3, which implied that the turbulence intensity is mainly affected by the geometry structure of the plates and pressure shows no evident influence. The integral scale $l_0$, which represents the mean size of the energy bearing vortex, and Kolmogorov scale $l_K$, corresponding to the smallest scale in turbulence, with respect to turbulence intensity $u'$ were shown in Fig. 4 and Fig. 5, respectively. The results show that $l_0$ increases as $u'$ at low intensity level, while it seems to reach a constant value when $u'$ is large. And it highly depends on the structure of the plates due the turbulence generation mechanism [22]. When looking at $l_K$, the character line of four plates collapse to a single curve, which indicates that the smallest scale in turbulence is only related to the fluctuations of the velocity field. Furthermore, smaller $l_K$ can be obtained at higher pressure, due to the significant change of the viscosity.

As the discussion on the composition of syngas in the earlier sections [5], we choose two $X_{CO}/X_{H2}$ ratios as 65/35 and 80/20. The rest of the components were represented by the "other component". In the current study, carbon dioxide $CO_2$ was regarded as the "other component" for the model syngas and the mole fraction is determined as $X_{OTHER}/(X_{CO} + X_{H2} + X_{OTHER}) = 3/10$ [5]. Moreover, $CH_4$/air flames were used to make the comparison. Table 2 listed the mole fractions of all components and Table 3 gave the properties of the tested mixture. The non-stretched laminar burning velocity $S_L$, which is a basic property of the mixture, was evaluated through the PREMIX module [23] in CHEMKIN-PRO [24] using the chemical kinetic model of GRI-Mech 3.0 [25]. Laminar flame thickness $\delta_L$ is calculated by $\delta_L = \alpha_D/S_L$ which is regarded as the diffusion thickness, with $\alpha_D$ represents the unburned gas thermal diffusivity. Markstein length $L_M$, which accounts for the dependence of local laminar flame speed on stretch rate, is the given by $L_M = \delta_L Ma$, with Markstein number expressed as $Ma$. Effective Lewis number $Le_{eff}$, accounts for the global thermal and mass diffusive ratio, and flame instability scale $l_i$, corresponds to the wave length of the peak growth rate, were also calculated [26,27] and listed in the Table.

## Results and discussions

### *Image processing*

Fig. 6 gives the direct image, the typical representative OH-PLF image, the flame front extracted from the OH distribution and the mean progress variable of the turbulent premixed flame, <c>. The strong illumination and the flame brush of turbulent premixed flames is clearly demonstrated by Fig. 6 (a),

**Table 1 – Perforated plates diameters and turbulence characteristics.**

| Plates. | Diameter (mm) | Open ratio (%) | Coefficient *a* | | Coefficient *b* | |
|---|---|---|---|---|---|---|
| | | | $u'$ | $R_\lambda$ | $u'$ | $R_\lambda$ |
| 21 | 2.1 | 60 | 0.034 | 3.582 | 0 | 8.978 |
| 35a | 3.5 | 65 | 0.067 | 11.309 | 0 | 4.620 |
| 40 | 4.0 | 55 | 0.090 | 14.340 | 0 | 7.390 |
| 35b | 3.5 | 40 | 0.151 | 22.408 | 0 | 30.125 |

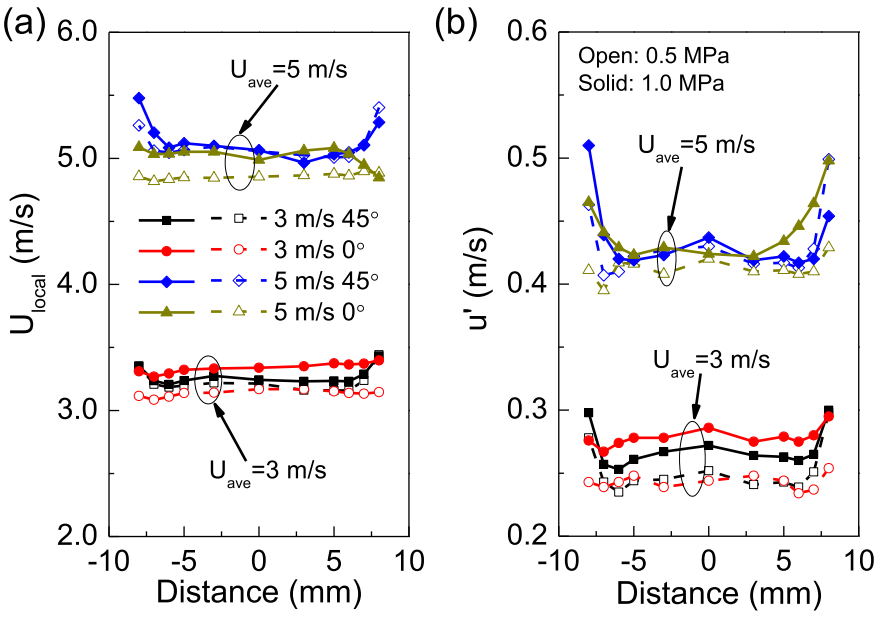


**Fig. 2 – Plots of $U_{local}$ and turbulence intensity $u'$ for Uave = 3.0 m/s and 5.0 m/s of plate 35b.**

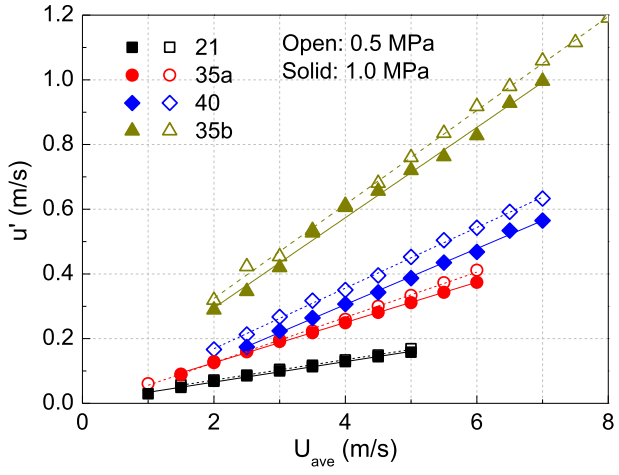


**Fig. 3 – Dependence of the turbulence intensity $u'$ upon $U_{ave}$.**

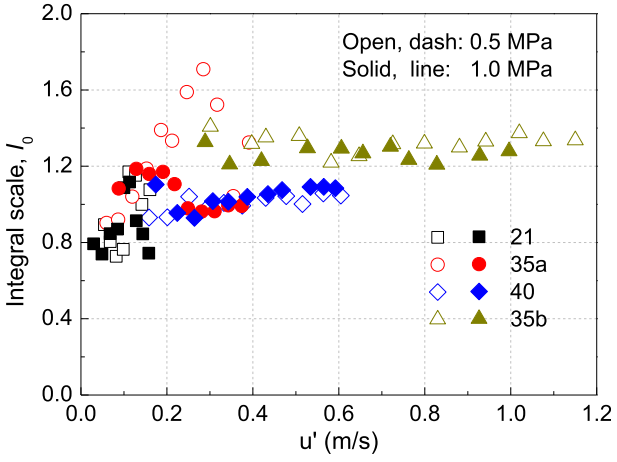


**Fig. 4 – Variation of the integral length scale, $l_0$, from different plates for 0.5 MPa and 1.0 MPa.**

however, it is a projection image which obtained from a long exposure time. Therefore, the digital image just provides the averaged information of the flame and the details such as the wrinkled structure cannot be illustrated. The OH-PLIF images under the same experimental conditions was shown in Fig. 6 (b). The corrugated flame interface can be well recognized with the distribution of the OH radical applying the adaptive threshold method to binarize the image for identifying wrinkled flame surface. Details of the flame image processing procedure were described in Refs. [17,28]. The turbulent mean progress variable <c> is a measuring of the progress in turbulent flame, from totally unburned gas <c> = 0 and completely burned gas <c> = 1. It can be obtained from the field of temperature, intermediate species, such as OH/$CH_2O$ distribution. In this study, 500 OH-PLIF images were averaged to obtain <c>. The leading edge, mean flame position and flame height of turbulent flame can be determined from the

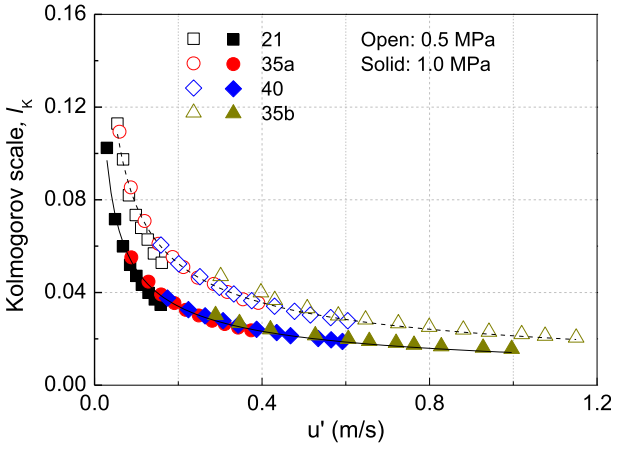


**Fig. 5 – Variation of the Kolmogorov length scale, $l_K$, from different plates for 0.5 MPa and 1.0 MPa.**

**Table 2 – Summary of mixture components mole fractions.**

| Mixtures | Components | $\phi$ | $X_{CO}$ | $X_{H2}$ | $X_{CH4}$ | $X_{CO2}$ | $X_{air}$ |
|---|---|---|---|---|---|---|---|
| CHA35 | CO/H2/CO2/air | 0.7 | 0.135 | 0.072 | – | 0.089 | 0.704 |
| CHA20 | CO/H2/CO2/air | 0.7 | 0.166 | 0.041 | – | 0.089 | 0.704 |
| CH4 | CH4/air | 1.0 | – | | 0.095 | – | 0.905 |

**Table 3 – Summary of properties of mixture and flames.**

| Mixtures | P (MPa) | $S_L$ (cm/s) | $\delta_L$ (mm) | $Le_{eff}$ | $L_M$ (mm) | $l_i$ (mm) |
|---|---|---|---|---|---|---|
| CHA35 | 0.5 | 18.44 | 0.0287 | 0.605 | 0.072 | 0.305 |
| CHA20 | 0.5 | 15.31 | 0.0315 | 0.720 | 0.086 | 0.408 |
| CH4 | 0.5 | 18.78 | 0.0245 | 1.048 | 0.100 | 0.652 |
| CHA35 | 1.0 | 13.49 | 0.0197 | 0.605 | 0.046 | 0.218 |
| CH4 | 1.0 | 13.35 | 0.0172 | 1.048 | 0.071 | 0.466 |

iso-contours of <c>, e.g. <c> = 0.1, 0.5 and 0.9, respectively, shown in Fig. 6 (d).

### *Flame front characteristics*

The information of the tested conditions were summarized in Table 4. Fig. 7 shows the Borghi's diagram [29], which divided turbulent flame to different combustion regimes. We can see

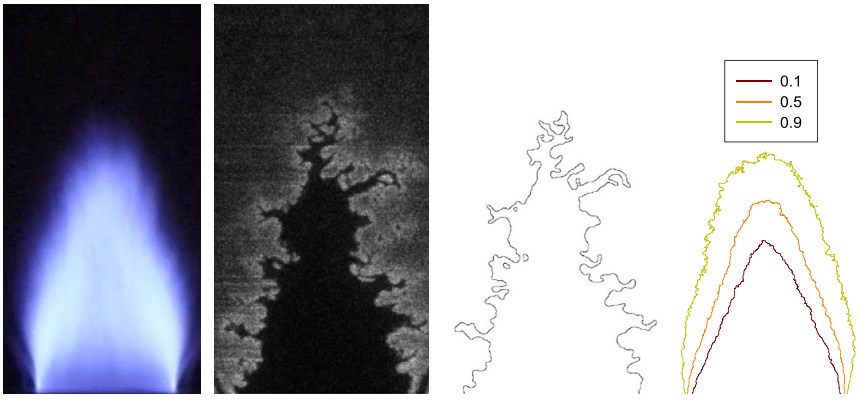


**Fig. 6 – (a) Direct digital image; (b) OH-PLIF image; (c) extracted flame front; (d) <c> contours from 500 images.**

**Table 4 – Turbulent velocities and equivalence ratios for the flames in this study.**

| Mixtures | XCO/XH2 | $\phi$ | P (MPa) | Abbre. | Plates | $S_L$ (cm/s) | $U_{ave}$ (m/s) | u' (m/s) | $R_\lambda$ |
|---|---|---|---|---|---|---|---|---|---|
| CO/H2/CO2/air | 65/35 | 0.7 | 0.5 | CHA35 | 21 | 18.44 | 3.0 | 0.102 | 19.7 |
| | 65/35 | 0.7 | 0.5 | CHA35 | 35a | 18.44 | 4.0 | 0.266 | 49.9 |
| | 65/35 | 0.7 | 0.5 | CHA35 | 40 | 18.44 | 4.0 | 0.360 | 64.7 |
| | 65/35 | 0.7 | 0.5 | CHA35 | 40 | 18.44 | 5.0 | 0.450 | 79.1 |
| | 65/35 | 0.7 | 0.5 | CHA35 | 40 | 18.44 | 6.2 | 0.558 | 96.3 |
| | 65/35 | 0.7 | 0.5 | CHA35 | 35b | 18.44 | 5.0 | 0.756 | 142.2 |
| | 65/35 | 0.7 | 0.5 | CHA35 | 35b | 18.44 | 6.0 | 0.907 | 164.6 |
| | 65/35 | 0.7 | 1.0 | CHA35 | 21 | 13.49 | 2.5 | 0.085 | 17.9 |
| | 65/35 | 0.7 | 1.0 | CHA35 | 40 | 13.49 | 2.5 | 0.225 | 43.2 |
| | 65/35 | 0.7 | 1.0 | CHA35 | 40 | 13.49 | 3.0 | 0.270 | 50.4 |
| | 65/35 | 0.7 | 1.0 | CHA35 | 40 | 13.49 | 4.0 | 0.360 | 64.7 |
| | 80/20 | 0.7 | 0.5 | CHA20 | 21 | 15.31 | 2.5 | 0.085 | 17.9 |
| | 80/20 | 0.7 | 0.5 | CHA20 | 35a | 15.31 | 3.3 | 0.220 | 41.9 |
| | 80/20 | 0.7 | 0.5 | CHA20 | 40 | 15.31 | 4.2 | 0.378 | 67.6 |
| | 80/20 | 0.7 | 0.5 | CHA20 | 40 | 15.31 | 5.2 | 0.468 | 82.0 |
| | 80/20 | 0.7 | 0.5 | CHA20 | 35b | 15.31 | 5.0 | 0.756 | 142.2 |
| CH4/air | – | 1.0 | 0.5 | CH4 | 21 | 18.78 | 2.0 | 0.068 | 16.1 |
| | – | 1.0 | 0.5 | CH4 | 21 | 18.78 | 3.0 | 0.102 | 19.7 |
| | – | 1.0 | 0.5 | CH4 | 35a | 18.78 | 4.0 | 0.266 | 49.9 |
| | – | 1.0 | 0.5 | CH4 | 40 | 18.78 | 3.0 | 0.270 | 50.4 |
| | – | 1.0 | 0.5 | CH4 | 40 | 18.78 | 4.0 | 0.360 | 64.7 |
| | – | 1.0 | 0.5 | CH4 | 35b | 18.78 | 3.4 | 0.514 | 106.3 |
| | – | 1.0 | 0.5 | CH4 | 35b | 18.78 | 4.2 | 0.635 | 124.2 |
| | – | 1.0 | 0.5 | CH4 | 35b | 18.78 | 6.0 | 0.907 | 164.6 |
| | – | 1.0 | 1.0 | CH4 | 21 | 13.35 | 2.5 | 0.085 | 17.9 |
| | – | 1.0 | 1.0 | CH4 | 40 | 13.35 | 3.0 | 0.270 | 50.4 |

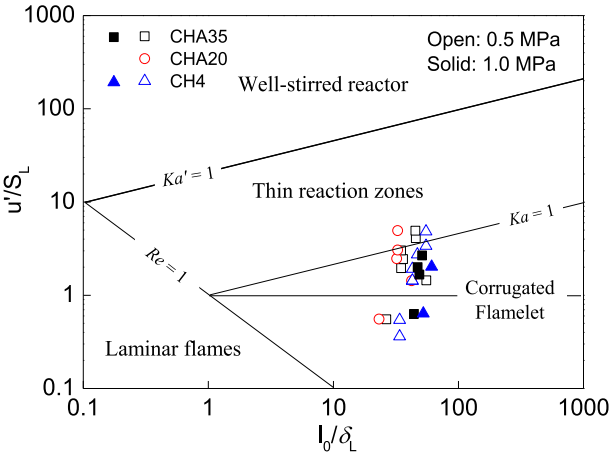


**Fig. 7 – Distribution of experimental conditions on the Borghi diagram.**

that the turbulent flames tested in this study were mostly located at flamelet regime, in which the flamelet concept can be implied here. Fig. 8 shows the representative OH-PLIF images of the aforementioned three flames at 0.5 MPa, with the sharp interface representing the flame front surface. It can be seen that the flame front was consisted by a large number of small scale concave/convex wrinkles which superimposed on large scale convex wrinkled structure. And the small wrinkled structure propagates deeply to the burned gas. The flames were presented at four different intensities which can interpret the role of hydrogen and the turbulence intensity effect. When the turbulence perturbation is small, say $u'/S_L \approx 0.6$, the wrinkled structure of syngas flames is more corrugated than $CH_4$/air flames. The cusp-like structure with very sharp pointed structure extending into the burned gas and wide rounded troughs towards the cold mixture is more frequently seen for syngas flames, resulting smaller front scale. This can be attributed to the influence of flame intrinsic instability on flame front structure, which results from the addition of

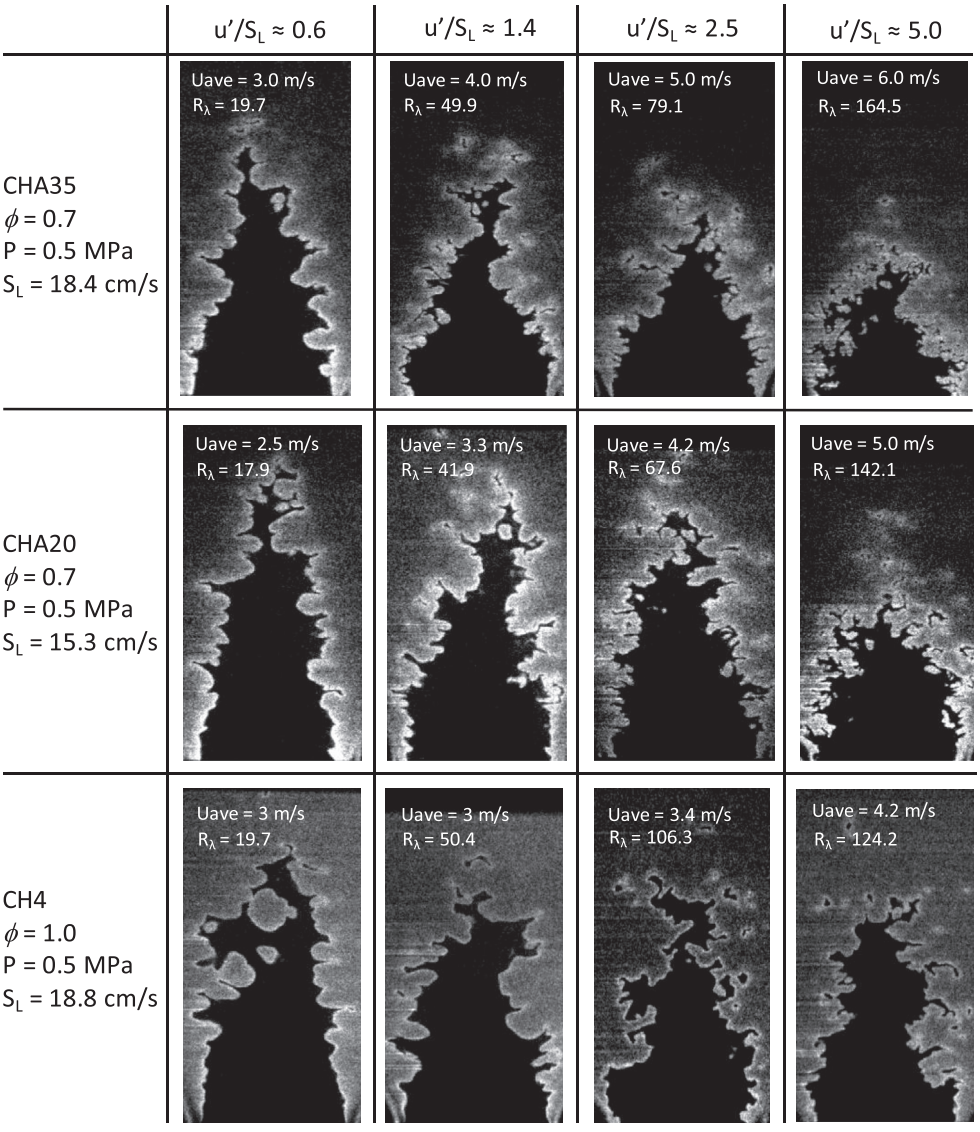


**Fig. 8 – Representative OH-PLIF images of the turbulent premixed flames under various conditions at P = 0.5 MPa.**

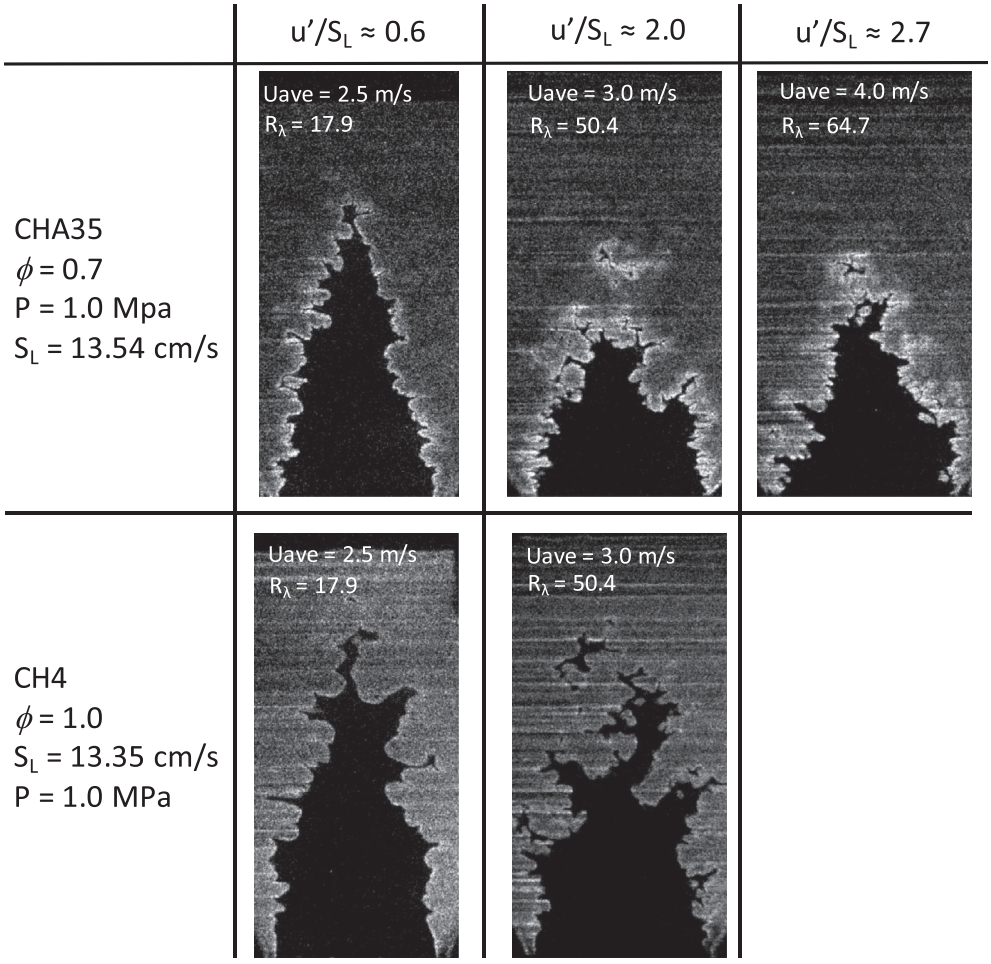


**Fig. 9 – Representative OH-PLIF images of the turbulent premixed flames under various conditions at P = 1.0 MPa.**

hydrogen and its properties discussed earlier. While, in the case of $CH_4$/air flames, the finger structure, which is an "elongated channels" filled by unburned gas in Ref. [30], are often generated, which will result in a larger spatial extension, namely a thicker turbulent flame brush and a larger flame volume. Moreover, hydrogen ratio in syngas can increase the intensity of this finer structure due to the fast burning property and instable effect of $H_2$, as embodied by Fig. 8. This is mainly due to the effective Lewis number $Le_{eff}$, which measures the unbalance of heat and mass diffusivity. As shown in Table 3, $Le_{eff}$ of syngas is much less than unity, implying there is a preferential diffusion, while no obvious preferential diffusion for $CH_4$/air mixtures since the effective Lewis number is close to unity. As the turbulence intensity increases, the flame tends to be shorter and the wrinkled structure tends to be much finer due to the smaller turbulent Kolmogorov length scale $l_K$, which mainly affect the small scale on the flame front. With even larger intensity, large amount of flame front was broken by the strong turbulent perturbation and developed frequently folds and isolated inlands filled with unburned mixtures that detach from the main flame surface and get rapidly consumed. And the effect of hydrogen is still evident on flame front structure. When the intensity is sufficiently high, say $u'/S_L \approx 5.0$, it is worth note that the flame topology or the characteristics of the wrinkled structure of CHA35/CHA20 and CH4 flames have apparently decreased to such an extent that it has no longer visible effect on the turbulent flames. We can conclude that the influence of the flame intrinsic instability on the wrinkled structure is weakened when largely increasing the pressure, as investigated and discussed by Peters [31] and Matalon [32]. Fig. 9 gave the OH-PLIF images for CHA35 and CH4 at 1.0 MPa. The wrinkled finer structure is more frequently seen compared to 0.5 MPa. The main reason is that flame thickness at higher pressure is thinner, which can result in stronger hydrodynamic instability. The pressure effect is more evident for the CHA35 flames under weak turbulence condition.

### *Flame surface density*

Flame surface density (FSD) measures the flame surface area in unit volume when the flamelet concept is applied, and it also can be approximated as the flame surface length per area in 2D measurement [17,33], which relates to the mean reaction rate as [34]:

$$\dot{\omega} = \rho_u \widetilde{S_L I_0} \Sigma = \rho_u \widetilde{S_{L,k}} \Sigma \quad (1)$$

where $\rho_u$ here is the density of unburned mixture, $I_0$ is the mean stretch factor, and $\Sigma$ represents FSD calculated with the

2D experimental OH-PLIF images. In experiment, the local FSD was obtained by measuring the flame length in a controlling box of 11 × 11 pixels, which has been tested as the optimal option [17,35]. The measured FSD is recorded in the center of controlling square which want through the whole flame region. The 2D data can be translated to the 3D flame surface density by taking the estimation models, as discussed in Ref. [33]. Fig. 10 and Fig. 11 show the local flame surface density, namely FSD field, corresponding to Figs. 8 and 9. First focusing on the results at 0.5 MPa, the FSD of the two model syngas flames is denser than that of CH4 flames. And the FSD of CHA35 is higher than CHA20, which is consistent with the flame corrugation shown in Fig. 8. Moreover, CH4 flame has a wider flame brush than the model syngas. The thinner flame brush and larger FSD would result in strong heat release which can may cause combustion oscillation. When looking at the results of 1.0 MPa, the FSD field has a similar trend as 0.5 MPa, while flame brush is further narrowed than the flames at 0.5 MPa, indicating that more intense combustion can be obtained by increasing the combustion pressure.

Fig. 12 shows the variation of conditional averaged FSD $\tilde{\Sigma}$ with mean progress variable <c> for different cases. The $\tilde{\Sigma}$ profile exhibits a symmetric shape and gets the peak value at about <c> = 0.5. Plots of the conditional averaged flame surface density always had a relation of

$$\tilde{\Sigma} = 4\tilde{\Sigma}_{max}\bar{c}(1-\bar{c}) \quad (2)$$

so that they would be typified by the maximum value. At 0.5 MPa, the $\tilde{\Sigma}_{max}$ of the two model syngas flames seems not depend on turbulence intensity or the ambient pressure. Moreover, $\tilde{\Sigma}$ profile of the two model syngas flames barely change when increasing turbulence intensity, while $\tilde{\Sigma}$ for CH4 flame increase slightly, which mainly due to the enhancement of the corrugated structures. At 1.0 MPa, CHA35 and CH4 flames at $u'/S_L \approx 2.0$ were shown. The $\tilde{\Sigma}_{max}$ and profiles of $\tilde{\Sigma}$ of CHA35 are almost identical to those at 0.5 MPa, while $\tilde{\Sigma}$ of CH4 is even larger than that of $u'/S_L \approx 3.0$ at the pressure of 0.5 MPa. The model syngas and CH4 flames shows a different behavior of $\tilde{\Sigma}$ , that turbulence intensity or pressure does not influence the flame surface density characteristics for model syngas while they highly affect that of CH4 flames. Moreover,

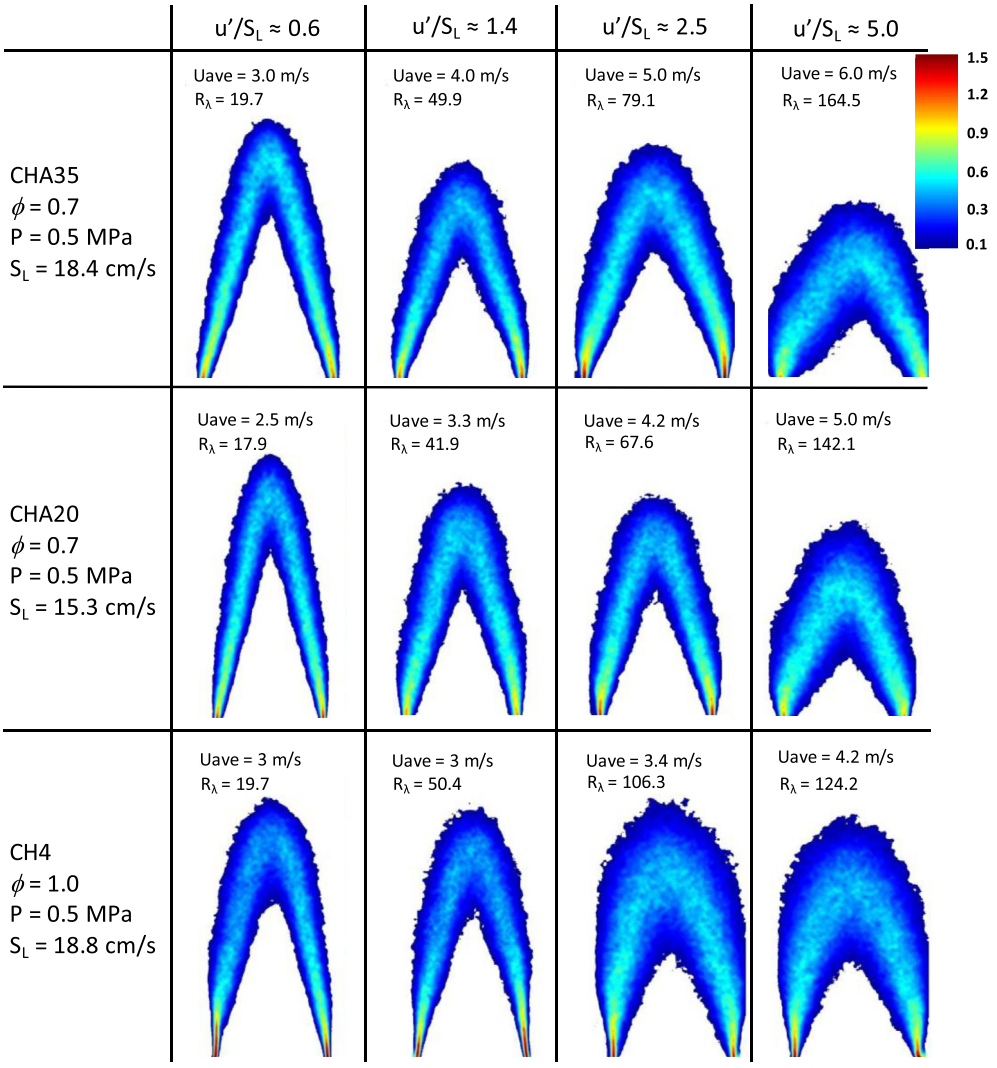


**Fig. 10 – Profiles of flame surface density corresponding to the flames in Fig. 8.**

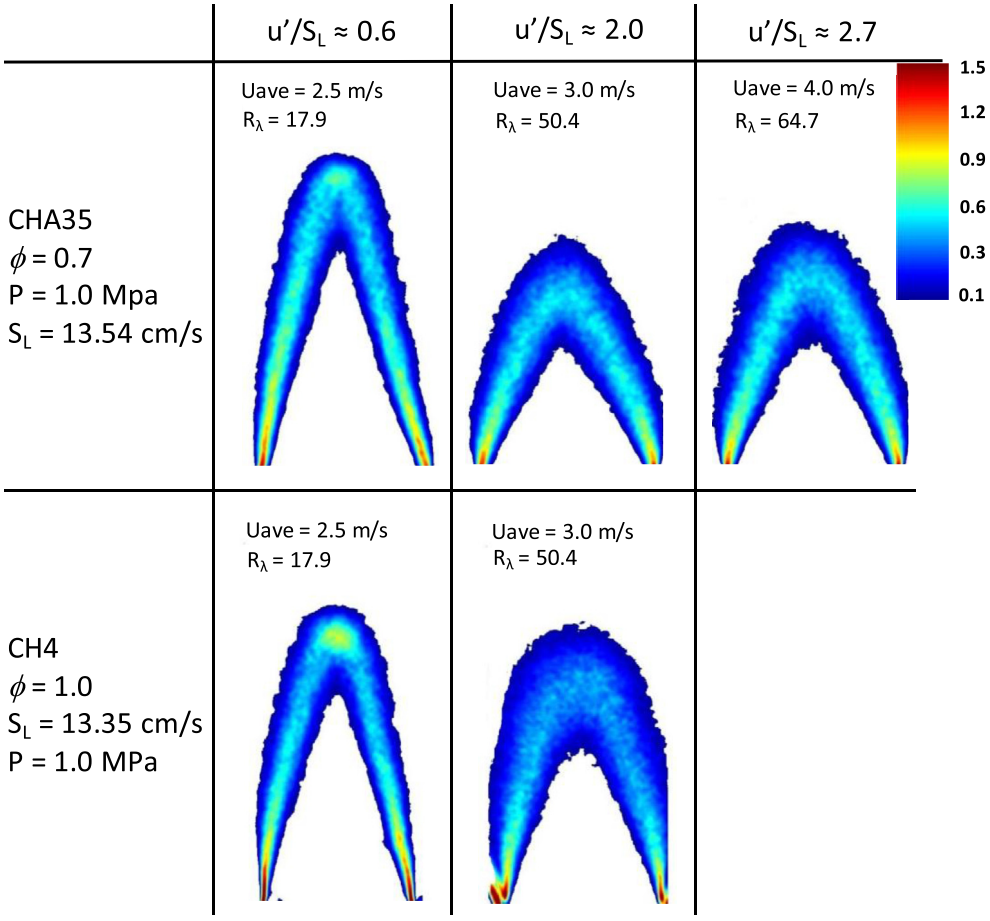


**Fig. 11 – Profiles of flame surface density corresponding to the flames in Fig. 9.**

hydrogen ratio has no evident effect on flame surface density for syngas Bunsen flames for both pressures.

To further illustrate the characteristics of $\tilde{\Sigma}$ of each flame investigated in current study, the relation of $\tilde{\Sigma}_{max}$ and the centerline flame brush thickness $\delta_T$ is plotted in Fig. 13 $\delta_T$ is defined as the distance between the cross point of burner axis and <c> = 0.1 and 0.9 contours [19], which is also an important parameter describing the spatial extension of the flame. The consumption speed of turbulent premixed flames $S_{T,c}/S_L$ can be calculated from Ref. [36].

$$S_{T,c}/S_L = \tilde{\Sigma}_{max}\delta_T I_0 \quad (3)$$

Therefore, the variation of $\tilde{\Sigma}_{max}$ with $\delta_T$ can be used to analysis the turbulent consumption speed. $\tilde{\Sigma}_{max}$ for CHA35 flame is slightly higher than that for CHA20, while much larger than CH4 flames, which has been discussed earlier. $\delta_T$ has no obvious effect on $\tilde{\Sigma}_{max}$ for all cases in the figure, even though the data is scattered. Moreover, the pressure does not influence $\tilde{\Sigma}_{max}$ for CHA35 flame, while it significantly enhances the $\tilde{\Sigma}_{max}$ for CH4 flame.

### *Turbulent burning velocity and flame volume*

Turbulent burning velocity $S_T/S_L$ is assumed to be a basic character of premixed turbulent combustion and it is of practical importance of determining the mean fuel consumption. $S_T$ in current study was calculated using a conventional angle method with <c> = 0.1, which is analogous to measure the laminar flame speed $S_L$ with a Bunsen burner [21]. The dependence of $S_T/S_L$ on $u'/S_L$ for the three tested flames was plotted in Fig. 14. $S_T/S_L$ significantly increases with $u'/S_L$ for all cases, due to the increase of the flame area resulted from wrinkled structure [37]. Moreover, we can see that the model syngas has a larger turbulent burning velocity than CH4 flames for both pressures of 0.5 MPa and 1.0 MPa. And due to the high diffusivity and fast burning property, $H_2$ addition significantly enhance $S_T/S_L$ and thus the increase of $S_T/S_L$ from CHA20 to CHA35 is evident, which can be observed from the flame front characteristics. It is clear seen from Table 3 that the main difference between the two syngas and CH4 under two pressures are $L_M$ and $l_i$. The equation below shows the relation of stretched flame speed $S_{L,k}$ and $L_M$ when encountered the local flame stretch $\alpha$,

$$S_L - S_{L,k} = \alpha L_M \quad (4)$$

where $S_{L,k}$ is local flame speed for stretched flame, $S_L$ is non-stretched laminar flame speed. Since the Markstein length for all flames in current work are all positive, the non-stretched laminar flame speed is suppressed by the flame stretch. $L_M$ of CH4 flame is 0.100, which is larger than the value

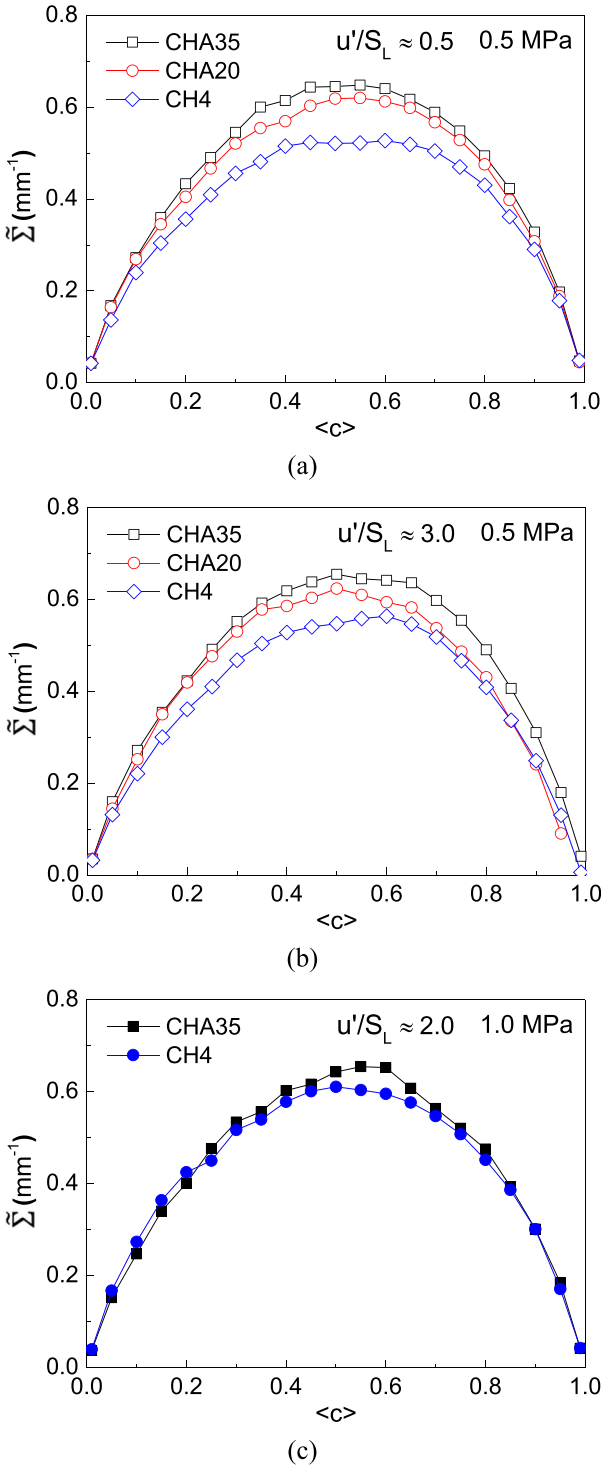


**Fig. 12 – Conditional averaged flame surface density against mean progress variable <c> at different conditions.**

of model syngas, and it decreases with hydrogen ratio, namely 0.086 and 0.072 for CHA20 and CHA35, respectively. When $L_M$ is large, the local burning velocity or flame speed will decrease more evidently with stretch rate encountered by the flame, which means the local flame surface responds more passively to the stretch.

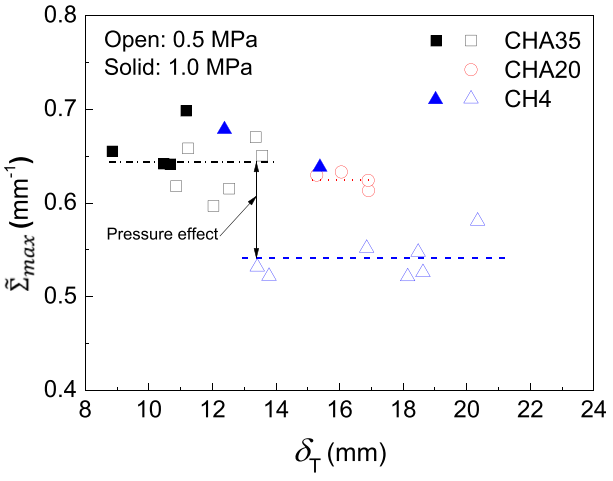


**Fig. 13 – Flame surface density as a function of flame brush thickness.**

Equation (3) shows the relation of the consumption speed, $\tilde{\Sigma}_{max}\delta_T$ and stretch factor $I_0$, with the latter representing an overall stretch effect on turbulent flame. Fig. 15 plots the variation of the turbulent burning velocity, which is considered as the equivalent consumption speed, and $\tilde{\Sigma}_{max}\delta_T$. This can be used to give an approximate measurement of $I_0$. It can be seen that $I_0$ is close to unity for all flames. Smaller $I_0$ is seen for CHA35 flame, which implies that local stretch has an overall suppression effect on turbulent combustion.

As mentioned earlier, the distribution of heat release intensity of the turbulent premixed flames relates to combustion oscillation in the premixed-type combustors, such as gas-turbine. Thus, turbulent flame region, where the flame front has possibility to show, was described by the mean volume $V_f$. The $V_f$ measures the three-dimensional volume inside the <c> = 0.1 and <c> = 0.9 iso-contours, which were fitted with a high order polynomial and then rotated 180° in the 2D approximation based on the isotropic assumption, as applied in Ref. [38]. The variation of $V_f$ was shown in Fig. 16 for both 0.5 MPa and 1.0 MPa. The $V_f$ is increasing with $u'/S_L$ at low

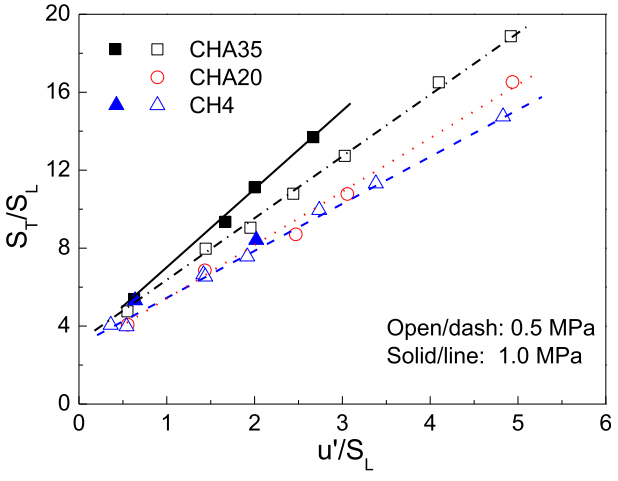


**Fig. 14 – Turbulent displacement speed and turbulent consumption speed with turbulence intensity.**

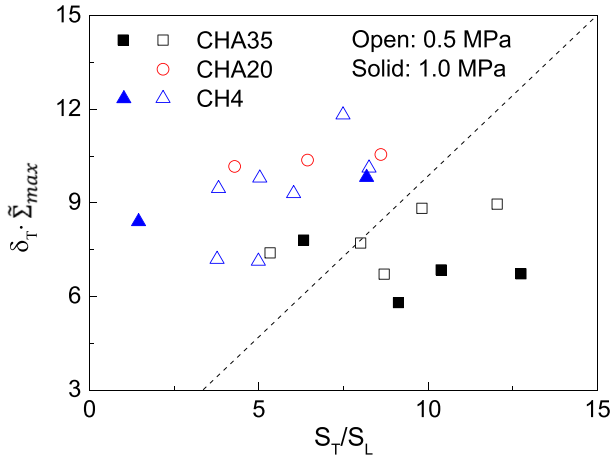


**Fig. 15 – Flame surface density multiplied by flame brush thickness as a function of the turbulence intensity.**

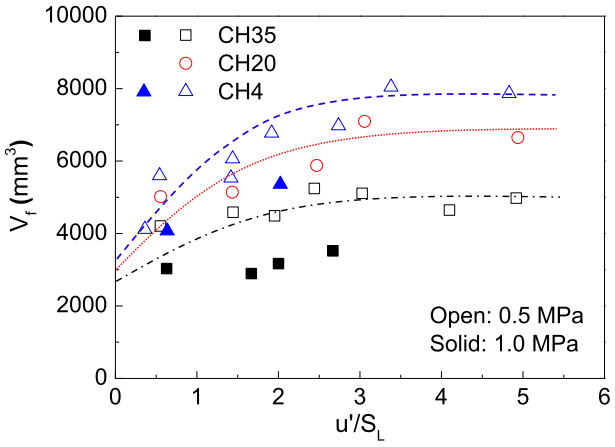


**Fig. 16 – Mean flame volume $V_f$ of turbulent premixed flames.**

intensity range and seems to level off when $u'/S_L$ is large for both pressures. And model syngas flames have a larger $V_f$ than the CH4 flames, which suggests that syngas flame would lead to a larger possibility to occur combustion oscillation. Several parameters may have an influence on the mean flame volume. One of them is the number and the size of the "elongated channels" on the flame front. It is important to recall that $V_f$ indicates the spatial region over which the flame fronts are located, thus longer "elongated channels" would lead to larger $V_f$. The increasing effect of the "elongated channels" on $V_f$ is only visible at low intensity which it is compensated by other factors at high intensity which needs to be further studied in the future.

## Conclusions

In order to investigate the turbulent combustion characteristics of lean syngas as well as the effect of hydrogen ratio at engine relevant conditions, flame front at high pressure up to 1.0 MPa was detected with OH-PLIF technique. A standard premixed turbulent Bunsen burner was utilized to stabilize the flame. A model syngas with two different $CO/H_2$ ratios, namely 65/35 and 80/20, at equivalence ratio of 0.7 and $CH_4$/air flame with equivalence ratio of 1.0 were tested. The model syngas was diluted with $CO_2$ to mimic the flue gas recycle. The turbulent flame front was statistically analyzed and quantitative parameters describing turbulent flame characteristics were obtained. Main conclusions are:

1. The high pressure turbulent premixed flames possess a character with small scale concave/convex structure superimposed on a large scale convex structure. The small scale concave structure propagates deeply to the burned side. The flame front of syngas flames is much finer and more corrugated than $CH_4$/air flames. The cusp-like structure with the very sharp pointed structure extending into the burned gas and large rounded troughs towards the cold mixture is more frequently seen for syngas flames, resulting smaller front scale. Hydrogen in syngas can increase the intensity of this finer structure.
2. The model syngas flames have larger flame surface density than $CH_4$/air flame. And higher hydrogen ratio in syngas can obtain higher flame surface density. This would due to the fact that syngas flames have smaller flame intrinsic instability scale $l_i$ than $CH_4$/air flame, which may generate smaller flame front scale and a weaken response of the local flame stretch against turbulence vortex motion.
3. The model syngas flames have larger turbulent burning velocity than CH4 flames both at 0.5 MPa and 1.0 MPa due to the high diffusivity and fast burning property. And the increase of $S_T/S_L$ from CHA20 to CHA35 is evident. This is mainly due to smaller $L_M$ and $l_i$. $V_f$ is much smaller for model syngas flames than that of $CH_4$ flames, which suggests that syngas flame would lead to a larger possibility to occur combustion oscillation.

## Acknowledgements

This study is supported by National Natural Science Foundation of China (No. 51706172, 51776164) and the Postal Doctoral Foundation of China (2017M613130). The authors greatly appreciated the valuable data provided by Prof. Hideaki Kobayashi from Tohoku University at Japan.

## REFERENCES

[1] Wall TF. Combustion processes for carbon capture. Proc Combust Inst 2007;31:31–47.
[2] Natarajan J, Kochar Y, Lieuwen T, Seitzman J. Pressure and preheat dependence of laminar flame speeds of H2/CO/CO2/O2/He mixtures. Proc Combust Inst 2009;32:1261–8.
[3] Sun ZY. Structure of turbulent rich hydrogen-air premixed flames. Int J Energy Res 2018;42:2845–58.
[4] Wang J, Zhang M, Xie Y, Huang Z, Kudo T, Kobayashi H. Correlation of turbulent burning velocity for syngas/air mixtures at high pressure up to 1.0 MPa. Exp Therm Fluid Sci 2013;50:90–6.

[5] Ichikawa Y, Otawara Y, Kobayashi H, Ogami Y, Kudo T, Okuyama M, et al. Flame structure and radiation characteristics of CO/H-2/CO2/air turbulent premixed flames at high pressure. Proc Combust Inst 2011;33:1543–50.
[6] Hannemann F, Koestlin B, Zimmermann G, Haupt G. Hydrogen and syngas combustion: pre-condition for IGCC and ZEIGCC. Siemens AG power generation, W8IN, G233; 2005.
[7] Brdar RD, Jones RM. GE IGCC technology and experience with advance gas turbines. Schenectady, NY: GE Power Systems, GER-4207; 2000.
[8] Wang J, Huang Z, Kobayashi H, Ogami Y. Laminar burning velocities and flame characteristics of CO–H2–CO2–O2 mixtures. Int J Hydrogen Energy 2012;37:19158–67.
[9] Hu EJ, Fu J, Pan L, Jiang X, Huang ZH, Zhang Y. Experimental and numerical study on the effect of composition on laminar burning velocities of H-2/CO/N-2/CO2/air mixtures. Int J Hydrogen Energy 2012;37:18509–19.
[10] Miao H, Lu L, Huang Z. Flammability limits of hydrogen-enriched natural gas. Int J Hydrogen Energy 2011;36:6937–47.
[11] Fu J, Tang C, Jin W, Thi LD, Huang Z, Zhang Y. Study on laminar flame speed and flame structure of syngas with varied compositions using OH-PLIF and spectrograph. Int J Hydrogen Energy 2013;38:1636–43.
[12] Sivaramakrishnan R, Comandini A, Tranter R, Brezinsky K, Davis S, Wang H. Combustion of CO/$H_2$ mixtures at elevated pressures. Proc Combust Inst 2007;31:429–37.
[13] Sung C-J, Law CK. Fundamental combustion properties of H2/CO mixtures: ignition and flame propagation at elevated pressures. Combust Sci Technol 2008;180:1097–116.
[14] Fairweather M, Ormsby MP, Sheppard CGW, Woolley R. Turbulent burning rates of methane and methane-hydrogen mixtures. Combust Flame 2009;156:780–90.
[15] Nakahara M, Shirasuna T, Hashimoto J. Experimental study on local flame properties of hydrogen added hydrocarbon premixed turbulent flames. J Therm Sci Technol 2009;4:190–201.
[16] Vreman AW, van Oijen JA, de Goey LPH, Bastiaans RJM. Direct numerical simulation of hydrogen addition in turbulent premixed Bunsen flames using flamelet-generated manifold reduction. Int J Hydrogen Energy 2009;34:2778–88.
[17] Zhang M, Wang J, Wu J, Wei Z, Huang Z, Kobayashi H. Flame front structure of turbulent premixed flames of syngas oxyfuel mixtures. Int J Hydrogen Energy 2014;39:5176–85.
[18] Guo HS, Tayebi B, Galizzi C, Escudie D. Burning rates and surface characteristics of hydrogen-enriched turbulent lean premixed methane-air flames. Int J Hydrogen Energy 2010;35:11342–8.
[19] Driscoll JF. Turbulent premixed combustion: flamelet structure and its effect on turbulent burning velocities. Prog Energy Combust Sci 2008;34:91–134.
[20] Wang J, Zhang M, Huang Z, Kudo T, Kobayashi H. Measurement of the instantaneous flame front structure of syngas turbulent premixed flames at high pressure. Combust Flame 2013;160:2434–41.
[21] Zhang M, Wang J, Xie Y, Jin W, Wei Z, Huang Z, et al. Flame front structure and burning velocity of turbulent premixed CH4/H2/air flames. Int J Hydrogen Energy 2013;38:11421–8.
[22] And EML, Livesey JL. Flow through screens. Ann rev fluid Mech 1978;10:247–66.
[23] Kee RJ, Grcar JF, Smooke MD, Miller JA, Meeks E. A ProgramforModeling steady, laminar, one-dimensional premixed flames. Albuquerque, NM: Sandia National Laboratories; 1985.
[24] Kee RJ, Rupley FM, Meeks E, Miller JA. A fortran chemical kinetics package for the analysis of gas- phase chemical and plasma kinetics. Albuquerque, NM: Sandia National Laboratories; 1993.
[25] Smith GP, Golden DM, Frenklach M, Moriarty NW, Eiteneer B, Goldenberg M, et al. GRI-Mech 3.0; 1999. http://www.me.berkeley.edu/gri_mech/.
[26] Bechtold JK, Matalon M. The dependence of the Markstein length on stoichiometry. Combust Flame 2001;127:1906–13.
[27] Yuan J, Ju YG, Law CK. On flame-front instability at elevated pressures. Proc Combust Inst 2007;31:1267–74.
[28] Wang J, Yu S, Zhang M, Jin W, Huang Z, Chen S, et al. Burning velocity and statistical flame front structure of turbulent premixed flames at high pressure up to 1.0 MPa. Exp Therm Fluid Sci 2015;68:196–204.
[29] Peters N. Turbulent combustion. Cambridge University Press; 2004.
[30] Lipatnikov AN, Chomiak J, Sabelnikov VA, Nishiki S, Hasegawa T. Unburned mixture fingers in premixed turbulent flames. Proc Combust Inst 2015;35:1401–8.
[31] Peters N, Wenzel H, Williams FA. Modification of the turbulent burning velocity by gas expansion. Proc Combust Inst 2000;28:235–43.
[32] Fogla N, Creta F, Matalon M. Effect of folds and pockets on the topology and propagation of premixed turbulent flames. Combust Flame 2015;162:2758–77.
[33] Zhang M, Wang J, Jin W, Huang Z, Kobayashi H, Ma L. Estimation of 3D flame surface density and global fuel consumption rate from 2D PLIF images of turbulent premixed flame. Combust Flame 2015;162:2087–97.
[34] Lee GG, Huh KY, Kobayashi H. Measurement and analysis of flame surface density for turbulent premixed combustion on a nozzle-type burner. Combust Flame 2000;122:43–57.
[35] Zhang M, Wang J, Xie Y, Wei Z, Jin W, Huang Z, et al. Measurement on instantaneous flame front structure of turbulent premixed CH4/H2/air flames. Exp Therm Fluid Sci 2014;52:288–96.
[36] Lawn CJ, Schefer RW. Scaling of premixed turbulent flames in the corrugated regime. Combust Flame 2006;146:180–99.
[37] Peters N. Laminar flamelet concepts in turbulent combustion. Proc Combust Inst 1986;21:1231–50.
[38] Kobayashi H, Hagiwara H, Kaneko H, Ogami Y. Effects of CO2 dilution on turbulent premixed flames at high pressure and high temperature. Proc Combust Inst 2007;31:1451–8.